Polarization-Modulated Rectification at Ferroelectric Surfaces

Weida Wu,[1,*] J. R. Guest,[2] Y. Horibe,[1] S. Park,[3] T. Choi,[1] S.-W. Cheong,[1] and M. Bode[2]

[1]*Rutgers Center for Emergent Materials and Department of Physics and Astronomy, Rutgers University, Piscataway, New Jersey, 08854, USA*

[2]*Center for Nanoscale Materials, Argonne National Laboratory, Argonne, Illinois 60439 USA*

[3]*Department of Physics, Chung-Ang University, Seoul, South Korea*

(Received 10 January 2010; published 24 May 2010)

By correlating room temperature conductive atomic force microscopy with low temperature electrostatic force microscopy images of the same sample region, we demonstrate that nanoscale electric conduction between a sharp tip and the surface of ferroelectric $HoMnO_3$ is intrinsically modulated by the polarization of ferroelectric domains. Conductance spectra reveal that the electric conduction is described by polarization-induced Schottky-like rectification at low bias, but dominated by a space-charge limited conduction mechanism at high bias. Our observation demonstrates visualization of ferroelectric domain structure by electric conduction, which may be used for nondestructive readout of nanoscale ferroelectric memories and/or ferroelectric sensors.

DOI: 10.1103/PhysRevLett.104.217601 PACS numbers: 77.80.Dj, 77.22.Jp, 77.55.Nv

Ferroelectric (FE) materials exhibit a characteristic transition temperature below which their broken inversion symmetry leads to a spontaneous electrical polarization. Because of their low cost and applicability nonvolatile high-density data storage, FEs have been utilized for thin film memory devices [1]. Often, the functionality of FE devices are compromised by charge conduction, i.e., leakage current, which is one of the technical bottlenecks for their practical application [2]. However, remarkable electronic transport properties have been reported recently in FE domains and domain walls of various ferroelectrics, revealing intriguing interplay between electronic properties and FE polarization [3–9]. In particular, the observation of a switchable diode effect in multiferroic $BiFeO_3$ single crystals indicates that the Schottky injection, beyond being a source of electric leakage, may also lead to a new way of controlling transport by FE polarization [5]. To date, however, most early studies have been performed with micrometer-sized planar devices, potentially complicating full reversible switching due to the presence of microscopic domains. Also, the symmetric electrode configuration leads to superposition of the contribution from both metal-FE interfaces [10,11].

In this Letter, we report on a combined electrostatic force microscopy (EFM) and conductive atomic force microscopy (cAFM) study on single crystalline FE $HoMnO_3$. By comparing data obtained at the same sample location but at different temperatures—below and above charge carrier freezing—we are able to directly demonstrate that the local Schottky-like rectification effect at the tip-surface junction is modulated by FE polarization of $HoMnO_3$. Additionally, we are able to show the crossover to a space-charge limited conduction (SCLC) mechanism at higher voltages in the conductance spectra for both up and down domains.

$HoMnO_3$ belongs to the family of improper FEs $RMnO_3$ (R = Ho, $\cdots$, Lu, Sc, and Y) where the ferroelectricity is driven by structural instability [12,13]. The optical band gap of this class of materials is approximately 1.5 eV [14–16]; as small band-gap FE semiconductors, they are appealing for technological applications with combined properties of semiconductors and FEs [17]. $HoMnO_3$ develops FE order below 875 K with a saturation polarization $P_Z \approx 5.5\ \mu C/cm^2$ along the c axis [9,18,19]. $HoMnO_3$ has been of particular interest because of its multiferroicity, i.e., the coexistence of (anti)ferromagnetism and ferroelectricity, the magnetoelectric coupling between them [20–22], and intriguing spin-rotation transitions [20,23]. At room temperature (RT), $HoMnO_3$ is a p-type semiconductor due to the presence of defects [24] and, therefore, the FE polarization is almost fully screened. Note that the RT resistivity of our $HoMnO_3$ samples [$\approx 10^5\ (\Omega \cdot cm)$] is much smaller than ionic resistivity due to oxygen vacancies [$>10^{14}\ (\Omega \cdot cm)$] with nominal diffusivity $\approx 10^{-18}\ cm^2/s$ [25]. Therefore, the primary carriers in $HoMnO_3$ are electronic in nature [4]. In contrast, at low temperatures, charge carriers in $HoMnO_3$ freeze-out and an unscreened FE polarization develops. As a result of this opposite trend in electrical conductivity and ferroelectric polarization, no local conduction ($\geq 10^{15}\Omega$) above the noise level was detected in c-AFM measurements below 200 K and a vanishing electrostatic signal was obtained in EFM measurements above 200 K. In order to correlate the FE domain structure with local conductance maps, EFM and cAFM images of the same surface area were obtained at 141 and 297 K, respectively. All experiments were performed under ultrahigh vacuum (UHV) and the sample was annealed at $\approx 150\,^\circ C$ overnight prior to the experiments to remove surface adsorbates.

Single crystal $HoMnO_3$ was grown by the floating zone method. For scanning probe microscopy (SPM) studies, the sample surface (001) was prepared by mechanical polishing, followed by annealing at ≈875 K to relax polishing strain. The surface is flat with roughness ≈3 nm. The SPM experiments were carried out in a commercial variable temperature UHV atomic force microscope or scanning tunneling microscope (VT-UHV-AFM/STM) system. EFM was carried out in noncontact mode with cantilever vibrating at its resonant frequency, while cAFM was performed in contact mode with commercial high performance current amplifier designed for STM (noise level is less than 10 fA at 3 GΩ gain). The AFM probes were Pt/Ir coated silicon cantilevers [26]. Samples for transmission electron microscopy (TEM) studies were prepared by Ar ion milling at liquid nitrogen temperature. A JEOL-2000FX and a JEOL-2010F TEM operating at 200 kV were used for the observations at RT.

Figure 1(a) shows a schematic illustration of the three-dimensional structure of FE domains in $HoMnO_3$ and the setup of the cAFM experiment. Surface FE domains are differentiated by their conductivity [shown in Figs. 1(d) and 1(f)] and extend into the bulk of the crystal. As shown in the perspective view of a cAFM image [Fig. 1(b)], the typical size of FE domains is ≈1 μm. The propagation of the FE domains along the c axis can be observed by RT TEM with the dark-field imaging technique by taking advantage of the failure of Friedel's law in noncentrosymmetric structures of ferroelectric materials [27,28], as shown in Fig. 1(c) [29]. The bright and dark contrasts represent 180° FE domains the size of which is in good agreement with FE domain size found in the cAFM image of Fig. 1(b). The directions of FE domain boundaries are meandering and not aligned with principle crystallographic orientations, which is also consistent with the absence of preferred FE domain boundary directions in the cAFM image.

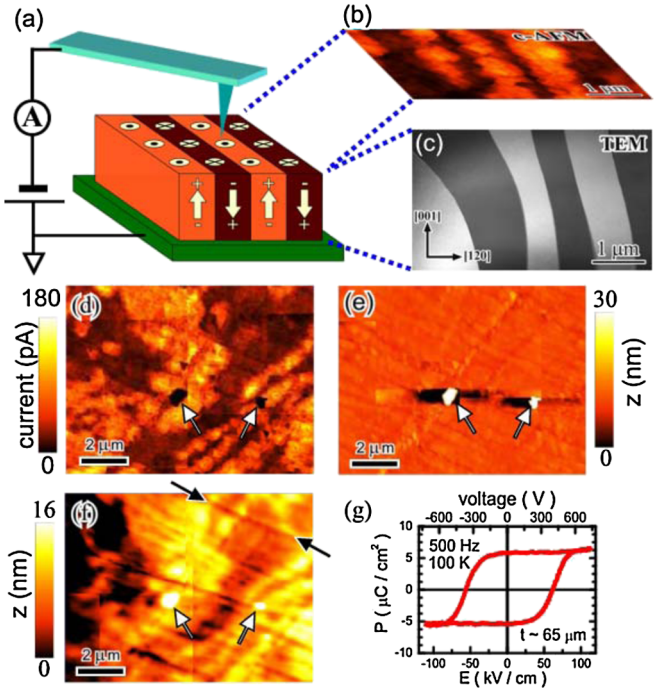

FIG. 1 (color online). (a) Schematic of the FE domains in $HoMnO_3$ and the setup of cAFM experiment. (b) Perspective view of a cAFM image. (c) RT TEM dark-field image of $HoMnO_3$ (side view). (d) cAFM and (e) topographic maps (10.3×7.9 μm^2) simultaneously measured at 297 K. (f) EFM map of the same location as (e) at 141 K. The imaging parameters are $V_{tip} = -3$ V ($V_{tip} = -6$ V) and $\Delta f = -10$ Hz ($F = 2$ μN) for EFM (cAFM). (g) P(E) loop measurement (of a different specimen with thickness ≈ 65 μm) at 100 K with 500 Hz.

Figures 1(d) and 1(f) are the comparison of the cAFM and EFM images taken at the same location of a single crystalline $HoMnO_3$(001) surface. In the EFM mode, the interaction between tip and sample surface is a superposition of the attractive van der Waals force and the electrostatic force. With negative tip bias, the bright contrast in EFM indicates stronger attractive interaction due to positive sample surface charges, i.e., domains with the polarization pointing up, while dark contrast indicates a weaker attractive interaction, i.e., polarization pointing down.

Because of some topographic cross-talk, a few line-shaped features originating from surface scratches due to polishing (one is indicated by black arrows) and two dust particles (white arrows) appear in the EFM image of Fig. 1(f) taken at 141 K. These topographic features served as alignment marks for subsequent RT cAFM imaging, as shown in Fig. 1(e). Comparing this FE domain pattern of Fig. 1(f) with the conduction map of Fig. 1(d) reveals an obvious correlation; at this bias voltage, up domains exhibit a larger local conduction than down domains. These results demonstrate that local conduction by cAFM can be a high resolution imaging mechanism for FE domains and defects. These correlations were observed at several locations on the sample and no change in topography and cAFM images was found before and after repeated cAFM scanning.

The origin of the contrast in cAFM images can be understood by comparing current-voltage (I-V) curves measured on up (blue) and down (green) domains [see Fig. 2(a)], where the inset of Fig. 2(a) shows the cAFM image with colored boxes indicating the areas where spatially averaged I-V curves are taken. In both domains, the I-V curves are nonlinear and dominated by the metal-semiconducting interface; the forward current 2 at negative tip bias is consistent with p-type character of the charge carriers in $HoMnO_3$ [30,31]. However, the rectification behavior is modulated by the FE polarization and therefore different for the two FE domains. While the rectification ratio is ≈60 for up domains at 10 V, it is ≈3 for down domains. Note that there is no hysteresis in the I-V measurements, suggesting negligible contribution from polarization switching and other extrinsic effects, e.g., oxygen vacancies.

To analyze the rectification behavior, the data in Fig. 2(a) are plotted semilogarithmically in Fig. 2(b). For bias values $|V_{tip}| < 3$ V, the forward current follows an exponential relationship with bias voltage suggesting the existence of a Schottky-like barrier at the tip-sample interface. The grey solid lines show exponential functions $I = I_S[\exp(eV/nk_BT) - 1]$, where e is the electron charge, k_B is the Boltzmann constant, T is the temperature, I_S is the saturation current, and n is a constant called the ideality factor, which is ≈ 40 from fitting. Such a large ideality factor is characteristic of highly doped or defective p-n junctions [32]. In this low-voltage range, up domains show lower conduction than down domains, suggesting a larger barrier formed at the tip-sample surface.

At higher bias ($|V_{tip}| > 5$ V), both forward and reverse currents are approximately proportional to V^2 as shown in Figs. 2(b) and 2(c). This is consistent with Child's law, suggesting a SCLC mechanism [30], which is a often observed in FEs [2] and is due to nonuniform injected charge density profile because of the poor conductivity of semiconductors. The intermediate voltage range (3 V $< |V_{tip}| < 5$ V) is indicated by arrows in Fig. 2(b) and defines the crossover between Schottky-like behavior at low bias and SCLC behavior at high bias. Interestingly, at forward current the transition from Schottky-like to SCLC is quite different for down and up domains. While the transition to a V^2 dependence occurs around -3 V bias [Fig. 2(c)] for down domains, up domains exhibit a more complicated behavior. Here, the forward current accelerates from -3 V until -5 V bias, exceeding the current value of down domains. In up domains, the characteristic V^2 dependence is observed for $V_{tip} < -5$ V [Fig. 2(c)]. This intriguing behavior leads to a local conduction contrast inversion between up and down domains as shown in I-V spectro-microscopy data from the $HoMnO_3$ surface shown in Fig. 2(d). This three-dimensional data set was obtained by measuring one I-V curve at every x, y position in the image; selected cAFM images are extracted for the indicated tip bias and displayed with the indicated current scaling. These local I-V properties are not strongly influenced by topography, which is shown for this sample region at the top of Fig. 2(d).

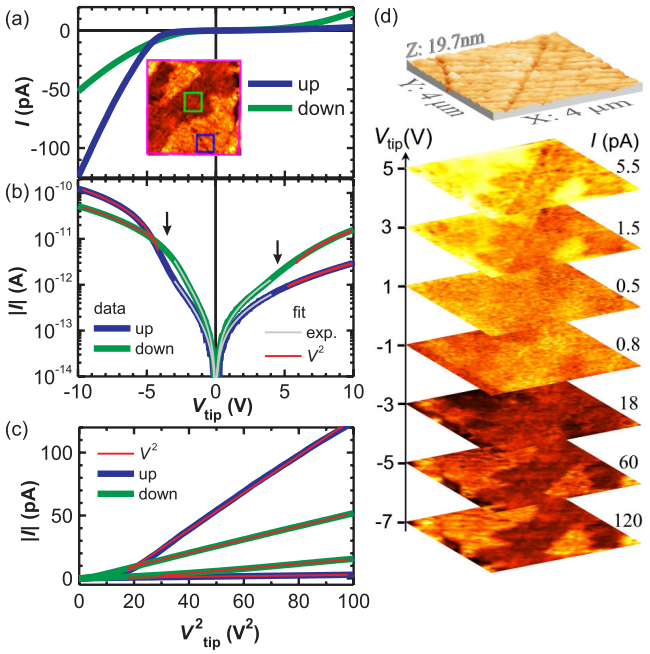

FIG. 2 (color online). (a) Spatially averaged I-V curves of up (blue) domain and down (green) domain from regions indicated by colored boxes in the inset, which shows a cAFM image at $V_{tip} = -6$ V. (b) Semilog plot of the data in (a). The grey solid lines show exponential fit functions for $|V_{tip}| < 3$ V, while the red solid lines show V^2 fit functions for $|V_{tip}| > 5$ V. The arrows indicate the crossover from Schottky-like to SCLC behavior. (c) I vs V^2 plot of the data in (a). The red solid lines are V^2 (linear) fits. (d) Topographic and cAFM images of $HoMnO_3$ surface taken with spectro-microscopic mode. (tip bias: -7 V to $+5$ V, indicated on the left axis). The image size is $\approx 4 \times 4$ μm^2. Note that bright contrast indicates larger absolute current value for $V_{tip} < 0$, while dark contrast indicates larger absolute current value for $V_{tip} > 0$. Current scales are listed on the right side of the individual images.

The different conduction properties at low bias of the two FE domains result from a Schottky-like barrier at the tip-sample interface which is modified by the local FE polarization [10,11]. This is illustrated in schematic interfacial band diagrams in Fig. 3 [30], where we have assumed that the work function of the semiconductor (ϕ_S) is larger than that of the metal (ϕ_M). The Schottky barrier (Φ_B) formed at the metal-semiconductor interface is a result of the work function mismatch. For FE semiconductors such as $HoMnO_3$, the presence of surface charge due to polarization bends the conduction (valence) band E_C (E_V) at the surface to maintain an uniform Fermi energy E_F (a.k.a. chemical potential), as shown in Fig. 3(a). Therefore, the Schottky barrier height Φ_B, formed when a metal is contacting the semiconductor, is modulated by the ferroelectric polarization P which produces surface charge with opposite sign on the different domains. Figure 3(b) shows the band bending diagram at zero bias.

The magnitude of the FE modulation of the Schottky-like barrier $\Delta\Phi_B$ can be estimated from the saturation current ratio at forward bias $I_S^{\downarrow}/I_S^{\uparrow} (\approx 1.3)$. Using a modified Schottky expression for the saturation current $I_S \propto \exp(-\Phi_B/nk_BT)$, this modulation takes the form $\Delta\Phi_B = (nk_BT)\ln(I_S^{\downarrow}/I_S^{\uparrow})$. Using the results from fits shown in Fig. 2(b), $\Delta\Phi_B \approx 0.27$ eV. This value is in good agreement with a simple dielectric gap model [10,11], $\Delta\Phi_B = P\delta/\epsilon_0\epsilon_{st} \approx 0.3$ eV, with realistic parameters ($P = 5.5$ μC/cm^2, $\delta \approx c = 1.1$ nm and $\epsilon_{st} \approx 20$ [18]).

As shown in Figs. 3(c) and 3(d), the Schottky barrier increases with increasing reverse bias ($V_{tip} > 0$), while it decreases with increasing absolute forward bias ($V_{tip} < 0$). Therefore, conduction in the forward direction is larger than in reverse, resulting in rectification. At high enough forward bias, the Schottky barrier will be fully suppressed,

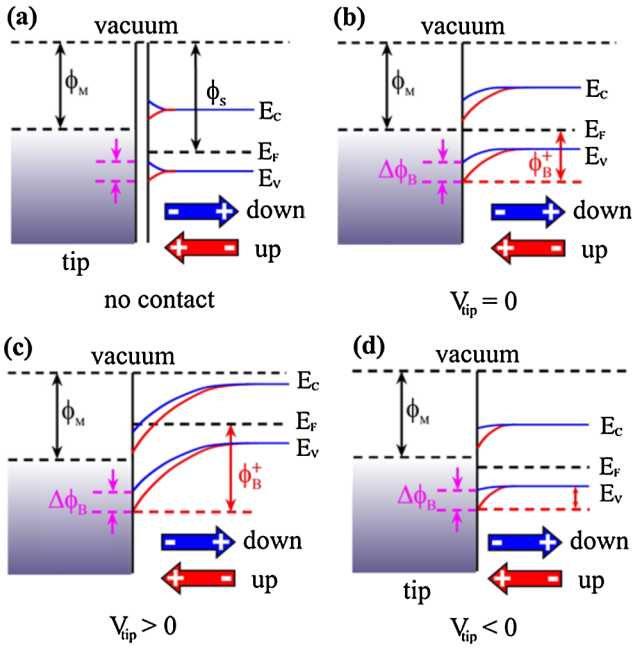

FIG. 3 (color online). Schematic diagrams of interfacial band diagram between cAFM tip and FE domains. ϕ_S (ϕ_M) is the work function of semiconductor (metal). E_C, E_V and E_F are energy level of conduction band, valence band and Fermi energy of semiconductor, respectively. (a) No contact between tip (metal) and sample (FE semiconductor). The presence of polarization bends the conduction (valence) band. (b) $V_{\text{tip}} = 0$ (zero bias); (c) $V_{\text{tip}} > 0$ (reverse bias); (d) $V_{\text{tip}} < 0$ (forward bias). Note that these diagrams are only applicable to low bias ($|V_{\text{tip}}| < 3$ V) behavior.

which may explain the crossover from Schottky-like to SCLC behavior. Our data show that the crossover voltage is larger for up domains than down domains, which is expected because up domains have a larger Schottky barrier to overcome in this system. Note that the Schottky-like barrier picture in band bending diagram (Fig. 3) is only applicable for low bias ($|V_{\text{tip}}| < 3$ V). Further studies, e.g., temperature dependence of *I-V* spectroscopy in conjunction with first principle calculations, will be carried out to reveal the exact nature of the metal-FE barrier at the $HoMnO_3$ surface.

In summary, we have demonstrated that nanoscale Schottky-like rectification is intrinsically modulated by the polarization of ferroelectric domains in multiferroic $HoMnO_3$ by correlating EFM and *c*-AFM images of the same sample location taken at different temperatures. Our observation demonstrates that this modulation effect can be used as a high resolution imaging mechanism of domains and nanoscale defects in small band-gap FE materials, and can also be harnessed for potential nanoscale multifunctional semiconductor devices, e.g., FE memories or sensors. These results open up possibilities of multiferroic electronics with multifunctionality, and should inspire further exploration of interplay of ferroelectricity, magnetism, and charge transport in small band-gap multiferroics.

We would like to thank David Vanderbilt and Karin Rabe for helpful discussions and input. This work was supported by NSF-DMR-0844807 and NSF-DMR-0520471. Use of the Center for Nanoscale Materials was supported by the U. S. Department of Energy, Office of Science, Office of Basic Energy Sciences, under Contract No. DE-AC02-06CH11357.

*wdwu@physics.rutgers.edu

[1] O. Auciello, J. Scott, and R. Ramesh, Phys. Today **51**, 22 (1998).
[2] M. Dawber, K. Rabe, and J. Scott, Rev. Mod. Phys. **77**, 1083 (2005).
[3] J. Seidel *et al.*, Nature Mater. **8**, 229 (2009).
[4] C.-H. Yang *et al.*, Nature Mater. **8**, 485 (2009).
[5] T. Choi *et al.*, Science **324**, 63 (2009).
[6] V. Garcia *et al.*, Nature (London) **460**, 81 (2009).
[7] P. Maksymovych *et al.*, Science **324**, 1421 (2009).
[8] A. Gruverman *et al.*, Nano Lett. **9**, 3539 (2009).
[9] T. Choi *et al.*, Nature Mater. **9**, 253 (2010).
[10] L. Pintilie and M. Alexe, J. Appl. Phys. **98**, 124103 (2005).
[11] L. Pintilie *et al.*, J. Appl. Phys. **98**, 124104 (2005).
[12] B. B. Van Aken *et al.*, Nature Mater. **3**, 164 (2004).
[13] S. W. Cheong and M. Mostovoy, Nature Mater. **6**, 13 (2007).
[14] J. Medvedeva *et al.*, J. Phys. Condens. Matter **12**, 4947 (2000).
[15] A. Souchkov *et al.*, Phys. Rev. Lett. **91**, 027203 (2003).
[16] W. Choi *et al.*, Phys. Rev. B **78**, 054440 (2008).
[17] V. Fridkin, *Ferroelectric Semiconductors* (Consultants Bureau, New York, 1980).
[18] G. Smolenskii and V. Bokov, J. Appl. Phys. **35**, 915 (1964).
[19] H. Tamura, E. Sawaguchi, and A. Kikuchi, Jpn. J. Appl. Phys. **4**, 621 (1965).
[20] B. Lorenz *et al.*, Phys. Rev. Lett. **92**, 087204 (2004).
[21] T. Lottermoser *et al.*, Nature (London) **430**, 541 (2004).
[22] S. Nandi *et al.*, Phys. Rev. Lett. **100**, 217201 (2008).
[23] O. Vajk *et al.*, Phys. Rev. Lett. **94**, 087601 (2005).
[24] G. Rao, B. Wanklyn, and C. Rao, J. Phys. Chem. Solids **32**, 345 (1971).
[25] R. Mogilevsky *et al.*, Phys. Rev. B **49**, 6420 (1994).
[26] Tip radius ≈30 nm, spring constant ≈40 N/m, resonant frequency ≈300 kHz, from Nanosensors (PPP-NCHPt) and BudgetSensors (TAP300E).
[27] F. Fujimoto, J. Phys. Soc. Jpn. **14**, 1558 (1959).
[28] M. Tanaka and G. Honjo, J. Phys. Soc. Jpn. **19**, 954 (1964).
[29] Taken with 036 reflection spot in electron diffraction based on the hexagonal space group of $P6_3cm$.
[30] S. M. Sze, *Physics of Semiconductor Devices* (John Wiley and Sons, Inc., New York, 1981).
[31] P. de Wolf *et al.*, J. Vac. Sci. Technol. **13**, 1699 (1995).
[32] J. Scott, Chem. Phys. Chem. **10**, 1761 (2009).